

Machine Learning for Ranking f-wave Extraction Methods in Single-Lead ECGs

Noam Ben-Moshe, Shany Biton, Kenta Tsutsui, Mahmoud Suleiman, Leif Sörnmo *Fellow, IEEE*, and Joachim A. Behar, *Senior Member, IEEE*

Abstract—Introduction: The presence of fibrillatory waves (f-waves) is important in the diagnosis of atrial fibrillation (AF), which has motivated the development of methods for f-wave extraction. We propose a novel approach to benchmarking methods designed for single-lead ECG analysis, building on the hypothesis that better-performing AF classification using features computed from the extracted f-waves implies better-performing extraction. The approach is well-suited for processing large Holter data sets annotated with respect to the presence of AF. Methods: Three data sets with a total of 300 two- or three-lead Holter recordings, performed in the USA, Israel and Japan, were used as well as a simulated single-lead data set. Four existing extraction methods based on either average beat subtraction or principal component analysis (PCA) were evaluated. A random forest classifier was used for window-based AF classification. Performance was measured by the area under the receiver operating characteristic (AUROC). Results: The best performance was found for PCA-based extraction, resulting in AUROCs in the ranges 0.77–0.83, 0.62–0.78, and 0.87–0.89 for the data sets from USA, Israel, and Japan, respectively, when analyzed across leads; the AUROC of the simulated single-lead, noisy data set was 0.98. Conclusions: This study provides a novel approach to evaluating the performance of f-wave extraction methods, offering the advantage of not using ground truth f-waves for evaluation, thus being able to leverage real data sets for evaluation. The code is open source (following publication).

Index Terms—f-wave extraction, atrial fibrillation, biomedical signal processing, machine learning, performance evaluation.

Manuscript submitted on July 18, 2023. The research was supported for NBM, SB, and JB by a grant (3-17550) from the Ministry of Science & Technology, Israel & Ministry of Europe and Foreign Affairs (MEAE) and the Ministry of Higher Education, Research and Innovation (MESRI) of France. SB, NBM, MS, and JAB acknowledge the support of the Technion-Rambam Initiative in Artificial Intelligence in Medicine, Hittman: Technion EVPR Fund: Hittman Family Fund and Israel PBC-VATAT and by the Technion Center for Machine Learning and Intelligent Systems (MLIS). (Corresponding author: jbehar@technion.ac.il)

N. Ben-Moshe, is with the Faculty of Computer Science and Faculty of Bio-Medical, Technion-IIT, Haifa, Israel.

S. Biton, and J. A. Behar are with the Faculty of Bio-Medical, Technion-IIT, Haifa, Israel.

M. Suleiman is with the Department of Cardiology, Rambam Medical Center and Technion The Ruth and Bruce Rappaport Faculty of Medicine, Haifa, Israel.

L. Sörnmo is with the Department of Biomedical Engineering, Lund University, Lund, Sweden.

K. Tsutsui is with the Department of Cardiovascular Medicine, Faculty of Medicine, Saitama Medical University International Medical Center, Saitama, Japan

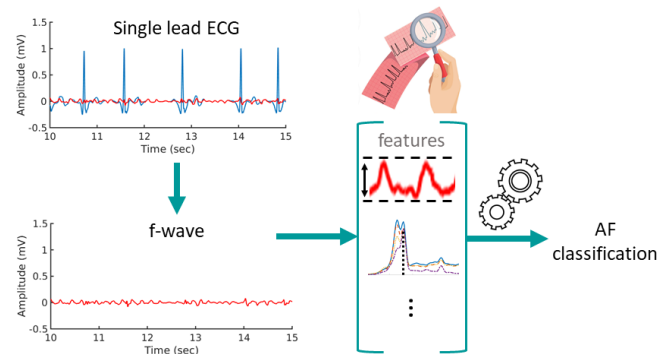


Fig. 1: An ECG is processed to estimate the f-wave using an extraction method. A set of f-wave features is used to train a machine learning model for AF classification. The performance of AF classification serves as a measure to rank the performance of different extraction methods. Part of the figure is adapted from Biorender.

I. INTRODUCTION

Fibrillatory waves (f-waves) are present in the ECG recorded from patients with atrial fibrillation (AF), representing the rapid and disorganized depolarization of the atria. Diagnosis of AF requires irregular RR intervals, absence of P-waves, and presence of f-waves. Therefore, f-wave information is important for diagnosis in order to distinguish AF from other arrhythmias such as atrial flutter (AFL) and multifocal atrial tachycardia.

Thanks to its simplicity, average beat subtraction (ABS) remains the most widely used f-wave extraction method in clinically oriented studies, building on the observation that atrial activity is decoupled from ventricular activity [1]. However, ABS suffers from several limitations due to the assumptions of the underlying model of stable QRS morphology and fixed noise level. Therefore, to offer better performance, several variants of ABS have been proposed [2]–[5], as well as blind source separation-based methods, including principal analysis [6], periodic [7], and independent component analysis [8]. Most of these methods assume that a multi-lead ECG is available.

The performance of f-wave extraction methods has been benchmarked by means of real as well as simulated ECG signals [1]. Depending on the type of signal, different local

TABLE I: Description of data sets. Age is presented as median and interquartile range (Q1–Q3).

| | UVAF | SHDB | RBDB |
|---------------|------------|------------|------------|
| Origin | USA | Japan | Israel |
| Patients, n | 100 | 100 | 100 |
| Age (yrs) | 69 (59–76) | 70 (62–75) | 70 (57–78) |
| Female, n_f | 50 | 45 | 50 |

measures have been used to quantify performance. For real ECGs, indirect measures have been used to quantify the large changes in f-wave amplitude which imply greater QRS residuals and poor f-wave extraction [9]–[11]. A disadvantage with such measures is their blindness to the spectral properties of the extracted signal, which are significant since the extracted signal typically exhibits a dominant frequency in the interval [4, 12] Hz.

For simulated ECGs, sample-by-sample measures quantifying the error between extracted and true f-wave signal has been used, e.g., in terms of the mean square error or the cross-correlation coefficient [5], [12], [13]. The use of simulated ECGs offers the advantage of having access to the ground truth, but, on the other hand, it comes with the disadvantage of not fully accounting for the physiological variability which exists across patients, neither for various types of real life noise and artifacts.

The standard 12-lead ECG continues to be used in clinical practice to diagnose AF, where lead V_1 offers the largest f-waves due to its proximity to the atria [14]. However, single-lead ECGs are becoming increasingly more common thanks to the development of patches and smartwatches for remote health monitoring and screening [15], [16]. Though single-lead ECGs cannot be used to confidently diagnose certain heart diseases, recent research has nonetheless shown that single-lead ECGs have a high clinical potential for detecting AF [17]–[21]. Since most research on f-wave extraction have assumed that multi-lead ECGs are available, there is an urgent need to develop methods for robust handling of single-lead ECGs.

The primary objective of the present study is to propose an approach to ranking of f-wave extraction methods designed for single-lead ECGs, whether real or simulated in nature. The approach builds on the hypothesis that better-performing AF classification using a set of features computed from the extracted f-waves implies better-performing extraction. The features are used as input to a machine learning model applied to successive, non-overlapping windows. The secondary objective is to investigate how the best-performing extraction method depends on lead position, age, and sex.

The paper is organized as follows. Section II describes the three real data sets consisting of Holter ECG recordings and the simulated data set. Section III describes the f-wave extraction methods subject to evaluation and the machine learning approach taken to AF classification. Section IV presents the performance on real and simulated data, followed by a discussion in Sec. V of the results and finally the conclusions in Sec. VI.

II. MATERIALS

A. Real data sets

Three different data sets were used: the University of Virginia Atrial Fibrillation data set (UVAF), USA [22], [23], the Rambam Hospital Holter clinic data set (RBDB), Israel [21], and the Saitama Hospital data set (SHDB), Japan [21]. UVAF consists of three-lead Holter recordings for which no lead information is available. The original data set consists of 2,147 patients totaling 51,386 hours of continuous ECG recordings. As no patient reports were available, the diagnoses were inferred from AF episode annotation [23]. RBDB consists of medical reports and three-lead Holter recordings (leads CM5, CC5, and CM5R), except when battery life had to be saved to handle recordings exceeding 24 h, then instead resulting in two-lead recordings (CM5 and CC5). SHDB consists of medical reports and two-lead Holter ECG recordings (leads NASA and CC5).

A subset of 100 recordings was used from each data set, similar to what was done in our previous work [21]. Briefly, stratification was performed according to age, sex, and AF diagnosis. Based on the cardiology report of each data set, 80 recordings were chosen from patients with AF. Each recording was manually reviewed and annotated with respect to AF episodes by an expert cardiologist [21]. Recordings were digitized at a sampling rate of 200 Hz. The median length of the recordings used in each data set was 24 h.

Each recording was divided in 1-min non-overlapping windows. Windows with mixed rhythms, defined as AF and non-AF rhythms, were excluded. The following two criteria were used to determine whether a window was to be excluded due to low signal quality: 1. the window contained too few QRS complexes (less than 10 QRS complexes), and 2. the signal quality index bSQI [24], [25] was below 0.8. In addition, windows annotated as AFL were excluded. The exclusion criteria were applied independently to each lead. Overall, 21% of all windows were excluded from the analysis. The number of windows in each lead and the number of excluded windows are listed in the supplement (Fig. S1).

B. Simulated data set

Two simulated data sets were generated using the model described in [26]. One data set was simulated without noise and the other with noise. The former set was simulated for the purpose of establishing an upper bound on performance, whereas the latter set was simulated as a mixture of baseline wander, muscle noise, and electrode movement artifacts, having a noise level of 100 μ V (root mean square, RMS) which can be viewed as representative of Holter recordings.

In each data set a total of 500 12-lead ECGs were simulated, all with a duration of about 5 min; lead V_1 was subject to analysis. Real components were used for simulation, i.e., ventricular rhythm, atrial activity (f- or P-waves), and QRST complexes were randomly chosen from different databases with real ECGs. The AF burden was chosen randomly from a uniform distribution defined by the interval [0, 1]. Each simulated recording was divided into windows in the same way as the real data sets.

III. METHODS

A. f-wave extraction

The ECG were filtered using a zero-phase, second-order bandpass filter, with a passband of 0.67–100 Hz to remove baseline wander [27] and high-frequency noise. Depending on data set, a notch filter at 50 or 60 Hz was used to remove powerline interference. Single-lead QRS detection was performed using the detector in [28].

We evaluate four different methods proposed for f-wave extraction [1], also suitable for the analysis of the fetal ECG in the presence of the maternal ECG [29], [30]. The code implementation is provided in the open resource fecgsyn.com [29]. The basic ABS method computes the ensemble average of time-aligned cardiac cycles, serving as a QRST template which is subtracted from the original ECG [31]. The resulting residual signal contains f-waves but also QRST-related residuals and noise. Variants of ABS offer different degrees of adaptability of the QRST template with respect to amplitude scaling. Either the entire QRST template is scaled by a factor before subtraction [32] or the QRS complex and the T-wave of the template are scaled individually [33]. These two methods are denoted ABS_{sc1} and ABS_{sc2}, respectively.

Using principal component analysis (PCA), the almost periodic characteristic of the ECG is explored for selective separation of the ventricular activity and the f-waves [34], see also [6]. This method performs eigenvector-based template subtraction (TS) and therefore denoted TS_{PCA}.

The extraction of f-waves is performed in every 1-min window and the resulting signal is denoted $d(n)$, $n = 1, \dots, N$, where N is the number of samples in the window. Examples of f-wave signals extracted using ABS, ABS_{sc1}, ABS_{sc2}, and TS_{PCA} are presented in Fig. 2.

B. f-wave features

A total of five features were computed, one defined in the time domain and four in the frequency domain. The *overall peak-to-peak amplitude* of the extracted f-wave signal is defined by

$$A_{pp} = \max_{n \in \Omega_f} (d(n)) - \min_{n \in \Omega_f} (d(n)), \quad (1)$$

where Ω_f is defined by all samples of $d(n)$, excluding those which are inside the QRS interval, whose limits are set 90 ms before and 90ms after the detected R-peak. The power spectrum of $d(n)$, denoted $P_d(\omega)$, was computed using Welch's method with a Hamming window and 50% segment overlap, see Fig. 3 for an example. The *dominant atrial frequency* (DAF) is defined by the position of the largest peak in the interval [4,12] Hz [1], corresponding to the normalized frequencies ω_l and ω_u , respectively,

$$\omega_{\text{DAF}} = \arg \max_{\omega_l \leq \omega \leq \omega_u} (P_d(\omega)). \quad (2)$$

Once ω_{DAF} is determined, the *DAF magnitude* is given by

$$P_{\text{DAF}} = P_d(\omega_{\text{DAF}}). \quad (3)$$

The *power inside the interval* [4,12] Hz and the *power outside the interval* are defined by

$$P_i = \int_{\omega_l}^{\omega_u} P_d(\omega) d\omega, \quad (4)$$

$$P_o = \int_0^{\omega_l} P(\omega) d\omega + \int_{\omega_u}^{\pi} P(\omega) d\omega, \quad (5)$$

respectively.

C. Machine learning

Based on the above five f-wave features, a random forest (RF) classifier was used to determine whether AF was present in 1-min windows. Classifier performance was measured by the area under the receiver operating characteristic (AUROC). Each of the four data sets were divided into a training set and a test set using a 80/20 split. For each training set and extraction method, a Bayesian search with a fivefold cross-validation was performed for hyperparameter tuning, using the search space given in Table II. The test sets were sampled 100 times and the AUROC was computed for each of the sampled sets. For each extraction method and data set the median was reported. The confidence interval of the AUROC was evaluated similar to [35].

TABLE II: Hyperparameter search space for grid search.

| Hyperparameter | Type | Range |
|----------------------|-------------|---------------------------|
| Number of estimators | Categorical | [100, 200, 300, 1000] |
| Max depth | Categorical | [1,2,3,4,5,6] |
| Max features | Categorical | [2, 6] |
| Max samples | Categorical | [0.1, 0.3, 0.5, 0.7, 0.9] |

D. Performance measures

In addition to the above-mentioned AUROC, used to evaluate classifier performance in both the real and the simulated data sets, another performance measure is used for simulated data sets which benefits from the availability of the ground truth f-waves. Since the main distinction among extraction methods lies in their ability to cancel the QRS complex, the RMS error is computed within the QRS interval, defined by 90 ms before and 90 ms after the R peak. The RMS error is also computed outside the QRS interval.

E. Statistical analysis

The f-wave features in windows classified as AF were analyzed by sex and age. The non-parametric Mann–Whitney rank test was used to determine whether the features were significantly different between men and women. $p < 0.05$ indicates a statistically significant difference. When evaluating features by age, the patients were divided into three age groups. The first group consisted of patients younger than 60 years old, the second group consisted of patients aged 60 or older but younger than 75, and the third group consisted of patients aged 75 or older.

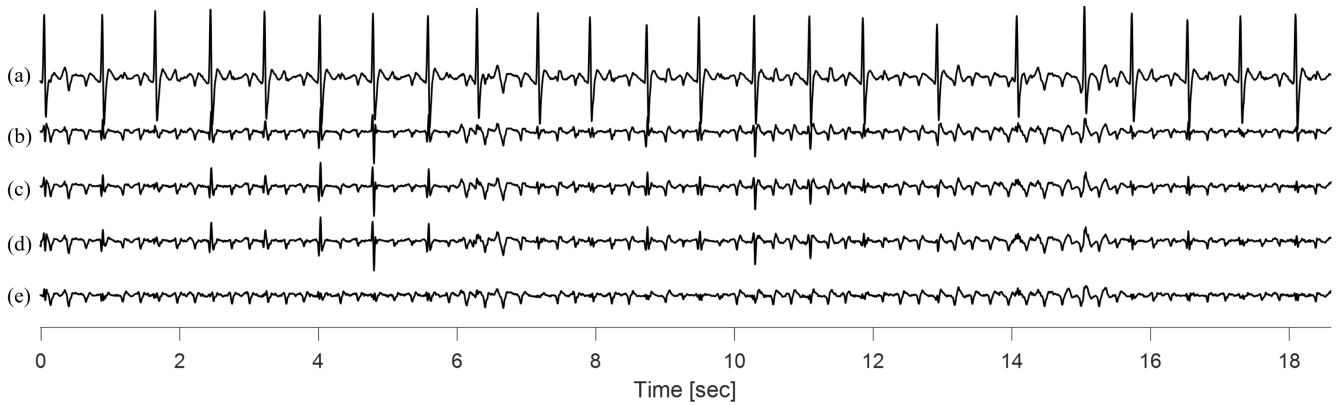


Fig. 2: Illustration of f-wave extraction. (a) A single-lead ECG with AF and related f-waves extracted using (b) ABS, (c) ABS_{sc1} , (d) ABS_{sc2} , and (e) TS_{PCA} . In this example, TS_{PCA} is associated with the smallest QRS-related residuals.

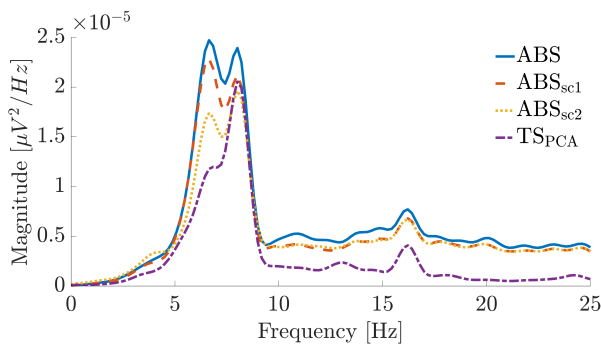


Fig. 3: Example of power spectrum for extracted f-wave signals obtained by the four different methods.

IV. RESULTS

A. Extraction performance on real data sets

Classifier performance is presented in Table III for each of the four extraction methods, each of the three data sets, and each of the two or three leads available. The results show that TS_{PCA} yielded the largest AUROC, regardless of the data set and lead analyzed.

Using TS_{PCA} , the largest AUROC is achieved for lead CM5R in RBDB and lead NASA in SHDB, i.e., 0.83 and 0.92, respectively, as these two leads are the ones nearest to the right atrium and with a vertical vector direction. Using TS_{PCA} , Fig. 4 illustrates f-wave extraction in different leads for ECGs excerpted from RBDB and SHDB. It should be noted that the lead with the largest AUROC for TS_{PCA} is also the one with the largest AUROC for the other three methods.

B. Extraction performance on a simulated data set

The AUROC obtained on the simulated data set are presented in Table IV for each of the four extraction methods when either noise-free or noisy ECGs are processed. While the four methods perform similarly on noise-free ECGs, the reduction in performance is more pronounced for the ABS-based methods than for TS_{PCA} when noisy ECGs are processed.

Table V presents the RMS error between extracted and true f-waves, computed either inside or outside the QRS interval.

TABLE III: Performance of AF classification on the three real data test sets, expressed in terms of area under the receiver operating characteristic (AUROC). For each extraction method and each lead, the median AUROC results are presented, where the best results are indicated by boldface.

| | UVAF | | | RBDB | | | SHDB | |
|-------------|-------------|-------------|-------------|-------------|-------------|-------------|-------------|-------------|
| | Ch1 | Ch2 | Ch3 | CM5 | CC5 | CM5R | CC5 | NASA |
| ABS | 0.69 | 0.75 | 0.78 | 0.65 | 0.60 | 0.81 | 0.86 | 0.87 |
| ABS_{sc1} | 0.76 | 0.79 | 0.81 | 0.62 | 0.63 | 0.80 | 0.85 | 0.88 |
| ABS_{sc2} | 0.76 | 0.76 | 0.81 | 0.63 | 0.60 | 0.82 | 0.86 | 0.88 |
| TS_{PCA} | 0.81 | 0.83 | 0.85 | 0.72 | 0.67 | 0.83 | 0.87 | 0.92 |

TABLE IV: Performance of AF classification on the simulated data sets, expressed in terms of the median AUROC.

| noise level (μ V RMS) | AUROC | |
|----------------------------|-------------|-------------|
| | 0 | 100 |
| ABS | 0.98 | 0.94 |
| ABS_{sc1} | 0.97 | 0.93 |
| ABS_{sc2} | 0.96 | 0.94 |
| TS_{PCA} | 0.99 | 0.98 |

The lowest RMS error inside the QRS interval is obtained for TS_{PCA} , being considerably lower than those of the ABS-based methods. As expected, the RMS error obtained outside the QRS interval is about the same for all four methods. Interestingly, TS_{PCA} produces a lower RMS error inside than outside the QRS interval for both noise-free and moderately noisy ECGs—a result which stands in contrast to the ABS-based methods.

C. Results across sex and age

Figure 5 presents the distributions of the five f-wave features as a function of sex, obtained on UVAF, RBDB, and SHDB. The results show that all features are significantly different between men and women. The medians of f-wave amplitude and spectral power of the DAF are lower in women than in men; this finding applies to all three data sets.

Figure 6 presents the distributions of the five f-wave features as a function of the three age groups. The results show that the youngest group, i.e. <60 years, exhibited higher medians compared to the other two groups.

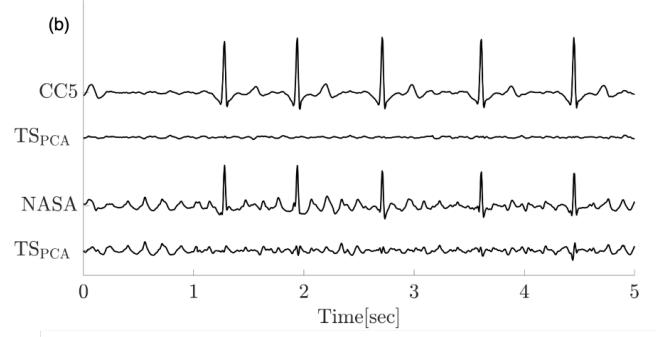
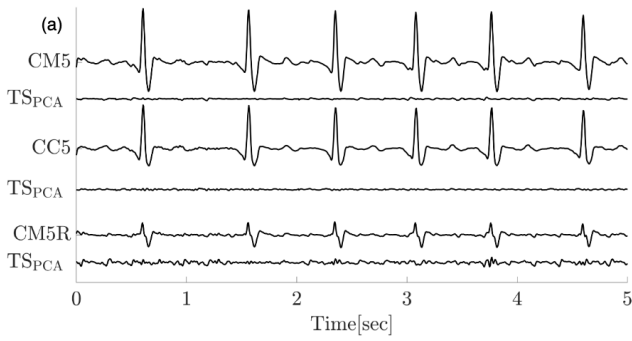


Fig. 4: Illustration of f-wave extraction in ECGs excerpted from (a) RBDB and (b) SHDB, using TS_{PCA} .

TABLE V: Performance of AF classification on the simulated data sets, expressed in terms of the RMS error between extracted and ground truth f-waves. The RMS error is computed inside and outside the QRS interval.

| noise level ($\mu\text{V RMS}$) | RMS error | | | |
|-----------------------------------|------------|-----------|-------------|-----------|
| | inside QRS | | outside QRS | |
| 0 | 0 | 0 | 0 | 0 |
| 100 | 16 | 30 | 11 | 27 |
| ABS | 12 | 27 | 10 | 27 |
| ABS_{sc1} | 13 | 27 | 10 | 27 |
| ABS_{sc2} | 8 | 25 | 10 | 16 |
| TS_{PCA} | | | | |

V. DISCUSSION

This study presents a novel approach to evaluating the performance of single-lead f-wave extraction methods, offering the distinct advantage of using large real data sets annotated with regard to the presence of AF. Another advantage is that the proposed approach does not measure performance in relation to the amount of QRS-related residuals as such measures run the risk of confusing a high noise level with large residuals. Yet another advantage is that the ranking of extraction methods is based on an AF classifier which takes into account the spectral properties of the f-waves.

The RF-based AF classifier was chosen because of its high accuracy and efficiency in handling large data sets. However, since the main purpose of the RF-based classifier is to rank f-wave extraction methods, but not necessarily to offer the best AF classification performance, some other technique like a support vector machine or XGBoost may just as well be used instead.

Of the four single-lead extraction methods evaluated, TS_{PCA} consistently performed the best across the three real data sets and different lead positions. For comparison, the performance was evaluated on two simulated data sets, with or without noise, supporting the result on the real data sets that TS_{PCA} performed better than the three ABS-based methods, expressed in terms of the AUROC as well as the RMS error between extracted and ground truth f-waves. As for ranking of the ABS-based methods, the AUROC varies across the real data sets and lead positions as well as across the simulated data sets, suggesting that these three methods offer similar performance.

In the present study, only a handful of well-known single-

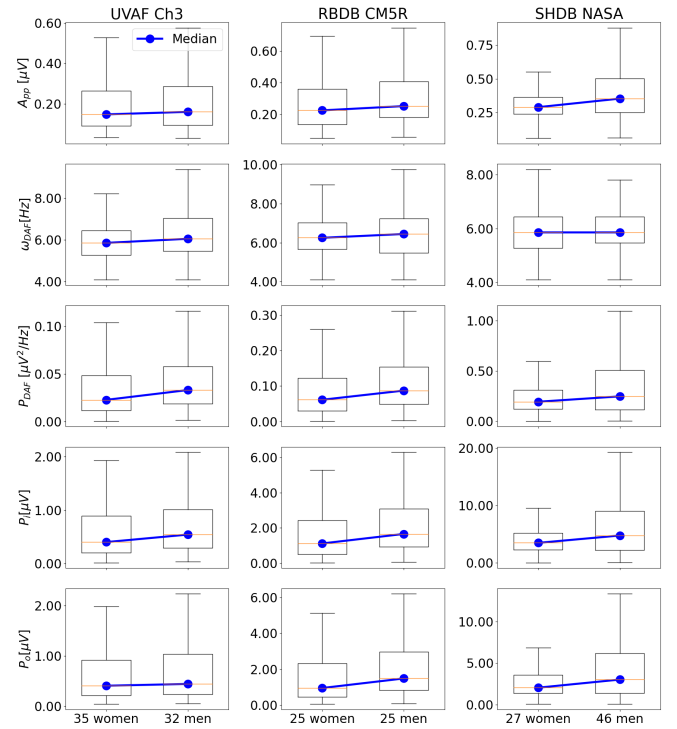


Fig. 5: Distributions of f-wave features as a function of sex, obtained on UVAF, RBDB, and SHDB. The first quartile, the median, and the third quartile are indicated by the box. The blue line is included to facilitate a comparison of women and men. The presented lead is selected based on the results presented in Table III.

lead extraction methods were evaluated. However, several other single-lead extraction methods would deserve to be evaluated, based on, e.g., modeling of the QRST complex and the f-waves in combination with an extended Kalman smoother [36], see also [29], resonance-based signal decomposition [37], and diffusion geometry data analysis expanding on the ABS principle [11].

The results vary with respect to lead position, showing that certain leads better capture the f-wave activity than others. Specifically, lead CM5R in RBDB and lead NASA in SHDB yielded the largest AUROC. Both these leads are roughly

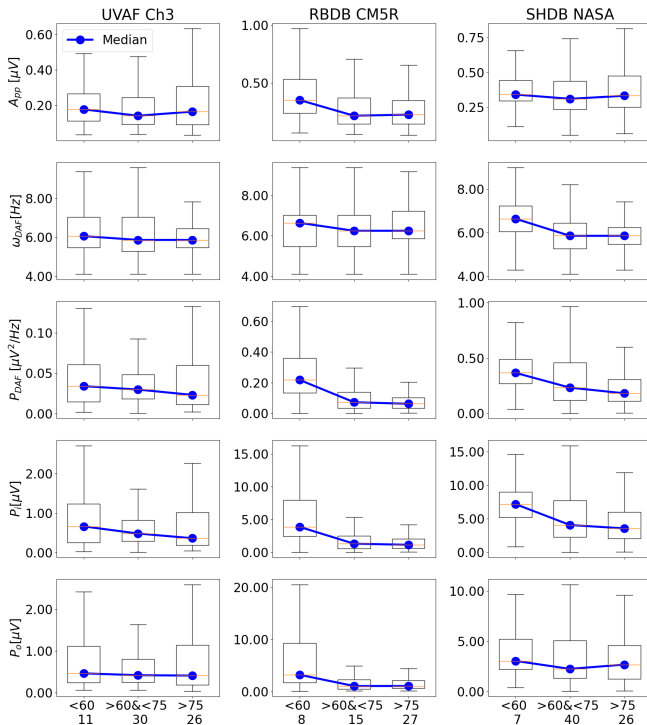


Fig. 6: Distributions of f-wave features as a function of age group, obtained on UVAF, RBDB, and SHDB, cf. Fig. 5 for explanation of the displayed information. The number of patients in each age group is indicated at the bottom of the figure.

positioned along the same axis relative to the electrical vector of the heart and positioned close to the right atrium, thus explaining why the f-waves are better captured in these leads than in the other leads of the data sets [14], [38]. Using the best-performing method, i.e., TS_{PCA} , and the lead associated with the largest AUROC of each real data set, and looking only at AF windows the distribution of the five f-wave features showed that men had higher median f-wave features values than women. It also showed that younger individuals had higher median f-wave features compared to older individuals.

Previous research has demonstrated that f-wave characteristics are associated with various clinical outcomes. For example, high f-wave amplitude is associated with a better prognosis in patients after AF ablation [39]. Low f-wave amplitude was shown to predict sinus node dysfunction following AF ablation in persistent AF [40]. Fine f-waves, defined by an amplitude less than 0.1 mV in all leads, is a risk factor for heart failure [41]. Evaluating the best f-wave extraction method using real ECGs can further strengthen research in cardiac electrophysiology by enabling a more precise f-wave characterization. For the clinical practice, single-lead f-wave extraction provides an opportunity to support the diagnosis of AF episodes by distinguishing AF from other supraventricular tachyarrhythmias and in those situations when AF is present but the heart rate is below 100 beats per minute. In addition, robust f-wave extraction could facilitate research on AF phenotypes that may be related to lead-dependent f-wave

manifestations.

As already noted, a limitation of the present study is that only a handful of extraction methods were subject to evaluation. However, the main aim of the study was to develop an approach for ranking of methods, and, therefore, the number of methods was kept low. Another limitation is the exclusion of atrial flutter windows, representing an important supraventricular tachyarrhythmia characterized by abnormal atrial activity, as well as mixed rhythms windows including both AF and non-AF beats. Since the F-waves in atrial flutter are more regular, the ranking of the extraction methods will most likely not be the same. Yet another limitation is that the groups divided into different sex or age were small. Therefore, a future study with larger groups will provide stronger and more conclusive results regarding f-wave characteristics. Since medication can influence the DAF as well as other f-wave characteristics, see, e.g., [42], medication should ideally be taken into account when evaluating f-wave characteristics. However, this information was only available in the RBDB and therefore not taken into consideration.

VI. CONCLUSIONS

This research offers a novel method for ranking of single-lead f-wave extraction methods based on AF classification performance. Four methods were evaluated on three real data sets from different geographical regions, where TS_{PCA} was ranked as the best-performing method. Robust extraction would facilitate more advanced research on f-wave characteristics and their association with clinical outcomes. The source code of this work is made open source to facilitate further research (upon publication).

REFERENCES

- [1] L. Sörnmo, A. Petrénas, P. Laguna, *et al.*, “Extraction of f waves,” in *Atrial Fibrillation from an Engineering Perspective*, Sörnmo L, Ed., Springer Nature, 2018, ch. 5, pp. 137–220.
- [2] H. Dai, S. Jiang, and Y. Li, “Atrial activity extraction from single lead ECG recordings: evaluation of two novel methods,” *Comput. Biol. Med.*, vol. 43, pp. 176–183, 2013.
- [3] E. Bataillou, E. Thierry, H. Rix, *et al.*, “Weighted averaging using adaptive estimation of the weights,” *Signal Process.*, vol. 44, pp. 51–66, 1995.
- [4] M. Stridh and L. Sörnmo, “Spatiotemporal QRST cancellation techniques for analysis of atrial fibrillation,” *IEEE. Trans. Biomed.*, vol. 48, pp. 105–111, 2001.
- [5] M. Lemay, J. M. Vesin, A. Van Oosterom, *et al.*, “Cancellation of ventricular activity in the ECG: Evaluation of novel and existing methods,” *IEEE. Trans. Biomed.*, vol. 54, pp. 542–546, 2007.
- [6] F. Castells, C. Mora, J. J. Rieta, *et al.*, “Estimation of atrial fibrillatory wave from single-lead atrial fibrillation electrocardiograms using principal component analysis concepts,” *Med. Biol. Eng. Comput.*, vol. 43, pp. 557–560, 2005.

- [7] S. Mihandoost, L. Sörnmo, M. Doyen, *et al.*, “A comparative study of the performance of methods for f-wave extraction,” *Physiol. Meas.*, vol. 43, 2022.
- [8] J. J. Rieta, F. Castells, C. Sánchez, *et al.*, “Atrial activity extraction for atrial fibrillation analysis using blind source separation,” *IEEE. Trans. Biomed.*, vol. 51, pp. 1176–1186, 2004.
- [9] R. Alcaraz and J. J. Rieta, “Adaptive singular value cancellation of ventricular activity in single-lead atrial fibrillation electrocardiograms,” *Physiol. Meas.*, vol. 29, pp. 1351–1369, 2008.
- [10] J. Lee, M. H. Song, D. G. Shin, *et al.*, “Event synchronous adaptive filter based atrial activity estimation in single-lead atrial fibrillation electrocardiograms,” *Med. Biol. Eng. Comput.*, vol. 50, pp. 801–811, 2012.
- [11] J. Malik, N. Reed, C.-L. Wang, *et al.*, “Single-lead f-wave extraction using diffusion geometry,” *Physiol. Meas.*, vol. 38, pp. 1310–1334, 2017.
- [12] E. K. Roonizi and R. Sassi, “An extended Bayesian framework for atrial and ventricular activity separation in atrial fibrillation,” *IEEE J. Biomed. Health Inform.*, vol. 21, pp. 1573–1580, 2017.
- [13] J. Mateo and J. J. Rieta, “Radial basis function neural networks applied to efficient QRST cancellation in atrial fibrillation,” *Comput. Biol. Med.*, vol. 43, pp. 154–163, 2013.
- [14] A. Petrénas, V. Marozas, and L. Sörnmo, “Lead systems and recording devices,” in *Atrial Fibrillation from an Engineering Perspective*, L. Sörnmo, Ed., Springer Nature, 2018, ch. 2, pp. 25–48.
- [15] S. R. Steinhubl, J. Waalen, A. M. Edwards, *et al.*, “Effect of a home-based wearable continuous ECG monitoring patch on detection of undiagnosed atrial fibrillation: The mSToPS randomized clinical trial,” *JAMA*, vol. 320, pp. 146–155, 2018.
- [16] P. M. Barrett, R. Komatireddy, S. Haaser, *et al.*, “Comparison of 24-hour Holter monitoring with 14-day novel adhesive patch electrocardiographic monitoring,” *Am. J. Med.*, vol. 127, pp. 11–95, 2014.
- [17] F. Kaasenbrood, M. Hollander, F. H. Rutten, *et al.*, “Yield of screening for atrial fibrillation in primary care with a hand-held, single-lead electrocardiogram device during influenza vaccination,” *Europace*, vol. 18, pp. 1514–1520, 2016.
- [18] E. Svennberg, M. Stridh, J. Engdahl, *et al.*, “Safe automatic one-lead electrocardiogram analysis in screening for atrial fibrillation,” *EP Europace*, vol. 19, pp. 1449–1453, 2017.
- [19] A. Chocron, J. Oster, S. Biton, *et al.*, “Remote atrial fibrillation burden estimation using deep recurrent neural network,” *IEEE. Trans. Biomed.*, vol. 68, pp. 2447–2455, 2021.
- [20] N. Ben-Moshe, S. Biton, and J. A. Behar, “Arnet-ECG: Deep learning for the detection of atrial fibrillation from the raw electrocardiogram,” in *Proc. Comput. Cardiol.* Vol. 49, 2022, pp. 1–4.
- [21] S. Biton, M. Aldhafeeri, E. Marcusohn, *et al.*, “Generalizable and robust deep learning algorithm for atrial fibrillation diagnosis across ethnicities, ages and sexes,” *NPJ Digit. Med.*, vol. 6, 2023.
- [22] S. S. Chugh, R. Havmoeller, K. Narayanan, *et al.*, “Worldwide epidemiology of atrial fibrillation: A Global Burden of Disease 2010 Study,” *Circulation*, vol. 129, pp. 837–847, 2014.
- [23] T. J. Moss, D. E. Lake, and J. R. Moorman, “Local dynamics of heart rate: detection and prognostic implications,” *Physiol. Meas.*, vol. 35, pp. 1929–1942, 2014.
- [24] J. Behar, J. Oster, Q. Li, *et al.*, “ECG signal quality during arrhythmia and its application to false alarm reduction,” *IEEE. Trans. Biomed.*, vol. 60, pp. 1660–1666, 2013.
- [25] Q. Li, Mark RG, and Clifford GD, “Robust heart rate estimation from multiple asynchronous noisy sources,” *Physiol Meas.*, vol. 29, pp. 15–32, 2008.
- [26] A. Petrénas, V. Marozas, A. Sološenko, *et al.*, “Electrocardiogram modeling during paroxysmal atrial fibrillation: application to the detection of brief episodes,” *Physiol. Meas.*, vol. 38, pp. 2058–2080, 2017.
- [27] P. Kligfield, L. S. Gettes, J. J. Bailey, *et al.*, “Recommendations for the standardization and interpretation of the electrocardiogram,” *Circulation*, vol. 115, pp. 1306–1324, 2007.
- [28] J. Pan and W. J. Tompkins, “A real-time QRS detection algorithm,” *IEEE. Trans. Biomed.*, vol. 32, pp. 230–236, 1985.
- [29] J. A. Behar, J. Oster, and G. D. Clifford, “Combining and benchmarking methods of foetal ECG extraction without maternal or scalp electrode data,” *Physiol. Meas.*, vol. 35, pp. 1569–1589, 2014.
- [30] J. Behar, F. Andreotti, S. Zaunseder, *et al.*, “A practical guide to non-invasive foetal electrocardiogram extraction and analysis,” *Physiol. Meas.*, vol. 37, R1–R35, 2016.
- [31] J. Slocum, A. Sahakian, and S. Swiryn, “Diagnosis of atrial fibrillation from surface electrocardiograms based on computer-detected atrial activity,” *J. Electrocardiol.*, vol. 25, pp. 1–8, 1992.
- [32] F. Beckers, W. Anné, B. Verheyden, *et al.*, “Determination of atrial fibrillation frequency using QRST-cancellation with QRS-scaling in standard electrocardiogram leads,” in *Proc. Comput. Cardiol.* Vol. 32, 2005, pp. 339–442.
- [33] S. M. M. Martens, C. Rabotti, M. Mischi, *et al.*, “A robust fetal ECG detection method for abdominal recordings,” *Physiol. Meas.*, vol. 28, pp. 373–388, 2007.
- [34] P. P. Kanjilal and G. Saha, “Fetal ECG extraction from single-channel maternal ECG using singular value decomposition,” *IEEE. Trans. Biomed.*, vol. 44, pp. 51–59, 1997.
- [35] S. Biton, S. Gendelman, A. H. Ribeiro, *et al.*, “Atrial fibrillation risk prediction from the 12-lead electrocardiogram using digital biomarkers and deep representation learning,” *Eur. Heart J. – Digital Health*, vol. 2, pp. 576–585, 2021.
- [36] R. Sameni, M. B. Shamsollahi, C. Jutten, *et al.*, “A nonlinear Bayesian filtering framework for ECG denois-

- ing.,” *IEEE. Trans. Biomed.*, vol. 12, pp. 2172–2185, 2007.
- [37] J. Zhu, J. Lv, and D. Kong, “f-wave extraction from single-lead electrocardiogram signals with atrial fibrillation by utilizing an optimized resonance-based signal decomposition method,” *Entropy*, vol. 24, 2022, Art. no. 812.
- [38] J. E. Waktare, M. M. Gallagher, A. Murtagh, *et al.*, “Optimum lead positioning for recording bipolar atrial electrocardiograms during sinus rhythm and atrial fibrillation,” *Clin. Cardiol.*, vol. 21, pp. 825–830, 1998.
- [39] S. Ishihara, M. Maruyama, T. Nohara, *et al.*, “Atrial fibrillatory wave amplitude revisited: A predictor of recurrence after catheter ablation independent of the degree of left atrial structural remodeling,” *Cardiol J.*, 2023.
- [40] A. Sunaga, M. Masuda, T. Kanda, *et al.*, “A low fibrillatory wave amplitude predicts sinus node dysfunction after catheter ablation in patients with persistent atrial fibrillation.,” *J. Interv. Card.*, vol. 43, pp. 253–261, 2015.
- [41] T. Kawaji, H. Ogawa, Y. Hamatani, *et al.*, “Association of inverted T wave during atrial fibrillation rhythm with subsequent cardiac events,” *Heart*, vol. 108, pp. 178–185, 2022.
- [42] D. Husser, M. Stridh, D. S. Cannom, *et al.*, “Validation and clinical application of time–frequency analysis of atrial fibrillation electrocardiograms,” *J. Cardiovasc. Electrophysiol.*, vol. 18, pp. 41–46, 2007.

VII. SUPPLEMENTARY SECTION

| | UVAF | | | RBDB | | | SHDB | |
|--------------------------------|-------------------|-------------------|-------------------|-------------------|-------------------|------------------|-------------------|-------------------|
| | Ch1 | Ch2 | Ch3 | CM5 | CC5 | CM5R | CC5 | NASA |
| All windows | 142,613 100% | 142,613 100% | 142,613 100% | 137,822 100% | 137,822 100% | 122,758 100% | 141,477 100% | 141,477 100% |
| After Signal Quality Exclusion | 131,447 92.17% | 129,298 90.66% | 118,840 83.33% | 114,942 83.40% | 113,355 82.25% | 98,299 80.08% | 139,326 98.48% | 138,737 98.06% |
| After AFL windows Exclusion | 129,925 91.10% | 127,776 89.60% | 117,318 82.26% | 109,957 79.78% | 109,061 79.13% | 93,314 76.01% | 137,197 96.97% | 136,608 96.56% |

Fig. S1: Exclusion criteria and number of windows excluded in each lead of each data set.